2014 IEEE International Conference on Robotics & Automation (ICRA)
Hong Kong Convention and Exhibition Center
May 31 - June 7, 2014. Hong Kong, China

Modeling of underwater snake robots

E. Kelasidi, K. Y. Pettersen, J. T. Gravdahl and P. Liljebäck

Abstract— **Increasing efficiency by improving the locomotion methods is a key issue for underwater robots. Hence, an accurate dynamic model is important for both controller design and efficient locomotion methods. This paper presents a model of the kinematics and dynamics of a planar, underwater snake robot aimed at control design. Fluid contact forces and torques are modeled using analytical fluid dynamics. The model is derived in a closed form and can be utilized in modern model-based control schemes. The proposed model is easily implemented and simulated, regardless of the number of robot links. Simulation results with a ten link robotic system are presented.**

I. INTRODUCTION

For centuries, engineers and scientists have gained inspiration from the natural world while searching for ideal solutions to technical problems. More recently, this process has been termed as biomimetics. Snake robots have been studied due to their ability to move in challenging environments, where other types of robots usually fail [1]. Empirical and analytical studies of snake locomotion were reported by Gray [2]. Among the first attempts to develop a snake prototype, the work of Hirose [3] is essential. The high number of DOFs of snake robots makes them difficult to control, but gives them the ability to traverse irregular environments, surpassing the mobility of conventional wheeled, tracked or legged robots [1].

Mobile robots continue to challenge researchers with new applications in a variety of environments [1]. The most recent fields of interest include the integration of robotic technology into underwater exploration, monitoring, and surveillance. Comparing amphibious snake robots to the traditional snake robots, the former ones have the advantage of adaptability to aquatic environments. The research on amphibious snake robots (also referred to as lamprey robots or eel-like robots) is, however, much less extensive, and fewer prototypes have been developed [4], [5], [6].

Increasing efficiency by improving the locomotion methods is a key issue for underwater robots. Increased agility and maneuverability are connected to a general decrease in the size of the robot, as well as more flexibility in its internal shape. In order to improve these properties, researchers begun studying aquatic biological systems and their methods of locomotion [7], [8], [9], [10].

There exist many underwater robots, and these can be classified into autonomous underwater vehicles (AUVs), remotely-operated underwater vehicles (ROVs), and bottom-crawling-legged underwater robots. More recently, there has been growing interest in the design, modeling and control of underwater robots that propel themselves and maneuver by mimicking the movement of a fish. A number of researchers have developed analytical models for the forces generated during the motion of these devices in the water [8].

The dynamics of snake robots moving on land have been derived by utilizing various modeling techniques [1]. The friction between the snake robot and the ground significantly affects its motion. In addition to many models of snake robots that consider sideslip constraints, there have been reported cases with anisotropic ground friction properties similar to biological snakes, providing the opportunity to model lateral undulation locomotion patterns. In [1], the authors provide an overview on modeling and analysis of snake robot locomotion emphasizing the growing trend toward locomotion in unknown and challenging environments. When it comes to swimming snake robots, only a few modeling approaches have been presented for eel-like robots [11], [12], [13]. Generally, studies of hyper-redundant mechanisms (HRMs), also known as snake robots, have focused on land based studies. An emerging field of study considers such multi-link systems suited for aquatic propulsion as well, and several prototypes of multi-link swimmers have been developed [5], [6], [11].

Two fundamental works in the field, of Taylor [9] and Lighthill [14], provide analytical models of fluid forces acting on the body during undulatory swimming. However, their analytical methods require a number of major simplifying assumptions. McIsaac and Ostrowski [11] presented a dynamic model of anguilliform swimming for eel-like robots and Boyer et al. [12] present the dynamic modeling of a continuous three-dimensional swimming eel-like robot. However, the majority of swimming robots modeling omit fluid moments which are supposed to have a negligible effect on the overall motion of the system [11], [15]. It should be noted that fluid moments are directly related to the power consumption of the system (see e.g. [13]) and thus, they are neglected in these modeling approaches in order to simplify the hydrodynamic effects. It is also worth noting that, in [13], [12] and [16] fluid moments are modeled, but the drag force and moment are integrated numerically at each sample time

E. Kelasidi, and J. T. Gravdahl are with the Department of Engineering Cybernetics at NTNU, NO-7491 Trondheim, Norway. E-mail: {Eleni.Kelasidi,Tommy.Gravdahl}@itk.ntnu.no

K. Y. Pettersen is with the Centre for Autonomous Marine Operations and Systems, Dept. of Engineering Cybernetics at NTNU, NO-7491 Trondheim, Norway. E-mail: Kristin.Y.Pettersen@itk.ntnu.no

Affiliation of P. Liljebäck is shared between the Dept. of Engineering Cybernetics at NTNU, NO-7491 Trondheim, Norway, and SINTEF ICT, Dept. of Applied Cybernetics, N-7465 Trondheim, Norway. E-mail: Pal.Liljeback@sintef.no.

This work was partly supported by the Research Council of Norway through project no. 205622 and its Centres of Excellence funding scheme, project no. 223254

of the algorithm and evaluated numerically, which results in the lack of a closed form solution. [17] presents the modeling of the reactive force and moment acting on an elongated body, moving in a weakly non-uniform potential flow. This model has been used to investigate the passive and the active swimming of a fish in a vortex street, while no viscous effects have been taken into account. In [18], a solution to the fast dynamics of eel-like robots has been proposed and tested in comparison with a Navier-Stokes solver. Furthermore, a number of research groups are currently working to develop accurate low-cost swimming models required for such problems [13].

In this paper we present a solution to the modeling problem that results in a closed form solution, avoiding the numerical evaluation of drag effects. In addition, it takes into account the current effect, using an analytical simplified form. For control design purposes, it is a main advantage that this hydrodynamic modeling concludes in a closed form, without the need of an algorithmic way to compute the drag force and torque and thus it is well suited for model-based control design of underwater snake robots locomotion. It is well known that the hydrodynamic forces (fluid forces) induced by the motion of a rigid body in an underwater environment are very complex and highly nonlinear and therefore several of these effects are often not taken into account when modeling the system. In this modeling approach, however, both the linear and the nonlinear drag forces (resistive fluid forces), the added mass effect (reactive fluid forces), the fluid moments and current effect are considered.

To the authors' best knowledge, this modeling approach is the first modeling approach that takes into account both the current effect and the combination of linear and nonlinear drag effect. It is important to notice that the ground snake robot model [19] falls out as a special case of the developed snake robot model, by replacing the fluid friction model with the ground friction model and setting the fluid parameters to zero. The presented model is thus an extension of the land based snake robot model [19], and comprise snake robots moving both on land and in water. In addition to providing completeness, this also makes the model applicable for unified control methods for amphibious snake robots moving both on land and in water.

This paper is organized as follows. Section II presents a 2D model of an underwater snake robot's kinematics and dynamics, explaining in detail the hydrodynamic effects, followed by simulations validations, for both serpentine and eel-like motions, in Section III. Conclusions and suggestions for future research are presented in Section IV.

II. MODELING OF UNDERWATER SNAKE ROBOTS

This section presents a continuous model of an underwater snake robot moving in the horizontal plane, i.e. moving at a constant depth. The snake robot is assumed to be neutrally buoyant, such that its depth stays constant unless active depth control (using rotation of the links around the body-fixed y-axis) is utilized. The model is derived for the purpose of analysis and design of motion control of the position and heading of the snake robot in this horizontal plane. The kinematics and dynamics of the robot taking into account the hydrodynamic effects will be presented.

A. Notations and defined symbols

The snake robot consists of n rigid links of equal length $2l, i = 1,\ldots,n$ interconnected by $n-1$ joints. The links are assumed to have the same mass m and moment of inertia $J = \frac{1}{3}ml^2$. The mass of each link is uniformly distributed so that the link CM (center of mass) is located at its center point (at length l from the joint at each side). The total mass of the snake robot is therefore nm. In the following sections, the kinematics and dynamics of the underwater snake robot will be modeled in terms of the mathematical symbols described in Table I and illustrated in Fig. 1a and Fig. 1b. Vectors are either expressed in the global coordinate system or in the local link coordinate system of link i. This is indicated by superscript *global* or *link,i*, respectively. If is not specified otherwise, a vector with no superscript is expressed in the global coordinate system. The following vectors and matrices are used in the subsequent sections:

$$\mathbf{A} = \begin{bmatrix} 1 & 1 & & \\ & \ddots & \ddots & \\ & & 1 & 1 \end{bmatrix}, \mathbf{D} = \begin{bmatrix} 1 & -1 & & \\ & \ddots & \ddots & \\ & & 1 & -1 \end{bmatrix},$$

where $\mathbf{A}, \mathbf{D} \in \mathbb{R}^{(n-1)\times n}$. Furthermore,

$$\mathbf{e} = \begin{bmatrix} 1 & \ldots & 1 \end{bmatrix}^T \in \mathbb{R}^n, \mathbf{E} = \begin{bmatrix} \mathbf{e} & \mathbf{0}_{n\times 1} \\ \mathbf{0}_{n\times 1} & \mathbf{e} \end{bmatrix} \in \mathbb{R}^{2n\times 2},$$

$$\sin\theta = \begin{bmatrix} \sin\theta_1 & \ldots & \sin\theta_n \end{bmatrix}^T \in \mathbb{R}^n, \mathbf{S}_\theta = \mathrm{diag}(\sin\theta) \in \mathbb{R}^{n\times n},$$

$$\cos\theta = \begin{bmatrix} \cos\theta_1 & \ldots & \cos\theta_n \end{bmatrix}^T \in \mathbb{R}^n, \mathbf{C}_\theta = \mathrm{diag}(\cos\theta) \in \mathbb{R}^{n\times n}$$

$$\mathrm{sgn}\theta = \begin{bmatrix} \mathrm{sgn}\theta_1 & \ldots & \mathrm{sgn}\theta_n \end{bmatrix}^T \in \mathbb{R}^n$$

$$\dot\theta^2 = \begin{bmatrix} \dot\theta_1^{\,2} & \ldots & \dot\theta_n^{\,2} \end{bmatrix}^T \in \mathbb{R}^n, \mathbf{J} = J\mathbf{I}_n, \mathbf{L} = l\mathbf{I}_n, \mathbf{M} = m\mathbf{I}_n$$

$$\mathbf{K} = \mathbf{A}^T\left(\mathbf{D}\mathbf{D}^T\right)^{-1}\mathbf{D}, \mathbf{H} = \left(\mathbf{I}_n - \frac{1}{n}\mathbf{e}\mathbf{e}^T\right)^{-1}\mathbf{K}^T, \mathbf{V} = \mathbf{A}^T\left(\mathbf{D}\mathbf{D}^T\right)^{-1}\mathbf{A}$$

The matrices $\mathbf{A}$ and $\mathbf{D}$ represent, respectively, an addition and a difference matrix, which will be used, for adding and subtracting pairs of adjacent elements of a vector. Furthermore, the vector $\mathbf{e}$ represents a summation vector, which will be used for adding all elements of a n-dimensional vector. The remaining vectors and matrices have been defined above since they are used in the model development.

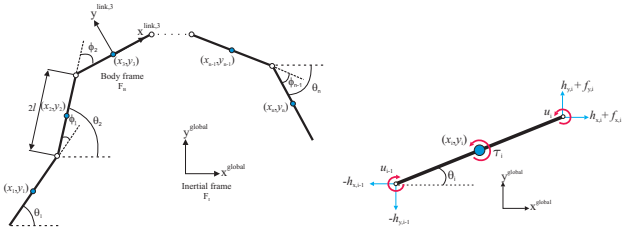

(a) Kinematic parameters (b) Forces and torques acting on each link

Fig. 1: Underwater snake robot

B. Kinematics of the underwater snake robot

The snake robot is assumed to move in a virtual horizontal and flat plane, fully immersed in water, and has n+2 degrees of freedom (n link angles and the x-y position of the robot). The *link angle* of each link $i \in 1,\ldots,n$ of the snake robot is denoted by $\theta_i \in \mathbb{R}$ and is defined as the angle that the link

TABLE I: Definition of mathematical terms

Symbol	Description	Vector
n	The number of links	
l	The half length of a link	
m	Mass of each link	
J	Moment of inertia of each link	
θ_i	Angle between link i and the global x axis	$\boldsymbol{\theta} \in \mathbb{R}^n$
ϕ_i	Angle of joint i	$\boldsymbol{\phi} \in \mathbb{R}^{n-1}$
(x_i, y_i)	Global coordinates of the CM of link i	$\mathbf{X}$,$\mathbf{Y} \in \mathbb{R}^n$
(p_x, p_y)	Global coordinates of the CM of the robot	$\mathbf{p}_{CM} \in \mathbb{R}^2$
u_i	Actuator torque of joint between link i and link $i+1$	$\mathbf{u} \in \mathbb{R}^{n-1}$
u_{i-1}	Actuator torque of joint between link i and link $i-1$	$\mathbf{u} \in \mathbb{R}^{n-1}$
$(f_{x,i}, f_{y,i})$	Fluid force on link i	$\mathbf{f}_x$,$\mathbf{f}_y \in \mathbb{R}^n$
τ_i	Fluid torque on link i	$\tau \in \mathbb{R}^n$
$(h_{x,i}, h_{y,i})$	Joint constraint force on link i from link $i+1$	$\mathbf{h}_x$,$\mathbf{h}_y \in \mathbb{R}^{n-1}$
$-(h_{x,i-1}, h_{y,i-1})$	Joint constraint force on link i from link $i-1$	$\mathbf{h}_x$,$\mathbf{h}_y \in \mathbb{R}^{n-1}$

forms with the global x axis with counterclockwise positive direction, while the *joint angle* of joint $i \in 1,\ldots,n-1$ is denoted $\phi_i \in \mathbb{R}$ and defined as

$$\phi_i = \theta_i - \theta_{i-1}. \tag{1}$$

The link angles and the joint angles are assembled in the vectors $\boldsymbol{\theta} = [\theta_1,\ldots,\theta_n]^T \in \mathbb{R}^n$ and $\boldsymbol{\phi} = [\phi_1,\ldots,\phi_{n-1}]^T \in \mathbb{R}^{n-1}$, respectively. The *heading* (or *orientation*) $\bar{\theta} \in \mathbb{R}$ of the snake is defined as the average of the link angles similar as for land-based snake robots in [19]

$$\bar{\theta} = \frac{1}{n}\sum_{i=1}^{n} \theta_i. \tag{2}$$

The model of the snake robot will be derived using link angles to simplify the mathematical expressions. The local coordinate system of each link is fixed in the CM of the link with x (tangential) and y (normal) axes oriented such that they are aligned with the global x and y axis, respectively, when all the link angles are zero. The rotation matrix from the global frame to the frame of link i is

$$\mathbf{R}^{\text{global}}_{\text{link},i} = \begin{bmatrix} \cos\theta_i & -\sin\theta_i \\ \sin\theta_i & \cos\theta_i \end{bmatrix}. \tag{3}$$

The global frame position $\mathbf{p}_{\text{CM}} \in \mathbb{R}^2$ of the CM (center of mass) of the robot is given by

$$\mathbf{p}_{\text{CM}} = \begin{bmatrix} p_x \\ p_y \end{bmatrix} = \begin{bmatrix} \frac{1}{nm}\sum_{i=1}^{n} m x_i \\ \frac{1}{nm}\sum_{i=1}^{n} m y_i \end{bmatrix} = \frac{1}{n}\begin{bmatrix} \mathbf{e}^T\mathbf{X} \\ \mathbf{e}^T\mathbf{Y} \end{bmatrix}, \tag{4}$$

where (x_i, y_i) are the global frame coordinates of the CM of link i, $\mathbf{X}= [x_1,\ldots,x_n]^T \in \mathbb{R}^n$ and $\mathbf{Y}= [y_1,\ldots,y_n]^T \in \mathbb{R}^n$. The forward velocity of the robot is denoted by $\bar{v}_t \in \mathbb{R}$ and is defined as the component of the CM velocity along the current heading of the snake, i.e.

$$\bar{v}_t = \dot{p}_x \cos\bar{\theta} + \dot{p}_y \sin\bar{\theta}. \tag{5}$$

The links are constrained by the joints according to

$$\mathbf{D}\mathbf{X} + l\mathbf{A}\cos\theta = \mathbf{0}, \quad \mathbf{D}\mathbf{Y} + l\mathbf{A}\sin\theta \quad = \mathbf{0}. \tag{6}$$

The position of the individual links as a function of the CM position and the link angles of the robot can be expressed as

$$\mathbf{X} = -l\mathbf{K}^T\cos\theta + \mathbf{e}p_x, \tag{7}$$
$$\mathbf{Y} = -l\mathbf{K}^T\sin\theta + \mathbf{e}p_y, \tag{8}$$

where $\mathbf{K} = \mathbf{A}^T\left(\mathbf{D}\mathbf{D}^T\right)^{-1}\mathbf{D} \in \mathbb{R}^{n\times n}$, and where $\mathbf{D}\mathbf{D}^T$ is nonsingular and thereby invertible [19]. The linear velocities of the links are found by differentiating the position of the individual links (7) and (8) with respect to time, which gives

$$\dot{\mathbf{X}} = l\mathbf{K}^T\mathbf{S}_\theta\dot{\theta} + \mathbf{e}\dot{p}_x, \quad \dot{\mathbf{Y}} = -l\mathbf{K}^T\mathbf{C}_\theta\dot{\theta} + \mathbf{e}\dot{p}_y. \tag{9}$$

The kinematics of an underwater snake robot is similar to that of a snake robot moving on land. In this section we provide a brief presentation of the kinematics for completeness. An extensive presentation of the snake robot kinematics can be found in [19]. Additionally, it is necessary to derive the equation of linear accelerations of the links in order to express the fluid forces in the following section. Hence, the linear accelerations of the links are found by differentiating the velocity of the individual links (9) with respect to time and using the second derivative of Eq. (4), which gives

$$\ddot{\mathbf{X}} = l\mathbf{H}\left(\mathbf{C}_\theta\dot{\theta}^2 + \mathbf{S}_\theta\ddot{\theta}\right), \quad \ddot{\mathbf{Y}} = l\mathbf{H}\left(\mathbf{S}_\theta\dot{\theta}^2 - \mathbf{C}_\theta\ddot{\theta}\right), \tag{10}$$

where $\mathbf{H} = \left(\mathbf{I}_n - \frac{1}{n}\mathbf{e}\mathbf{e}^T\right)^{-1}\mathbf{K}^T \in \mathbb{R}^{n\times n}$, and where $\mathbf{I}_n - \frac{1}{n}\mathbf{e}\mathbf{e}^T$ is nonsingular and thereby invertible.

C. Hydrodynamic modeling

As has been noted in the bio-robotics community, underwater snake (eel-like) robots bring a promising prospective for improving the efficiency and maneuverability of modern-day underwater vehicles. However, it should be mentioned that, for swimming robots, the dynamic modeling of the contact forces is most complicated compared to the modeling of the overall rigid motion and the dynamics of the body deformation. Hence, the hydrodynamic modeling task presents a major challenge. In addition, the validity of Taylor's resistive [9] and Lighthill's reactive [14] model assumptions varies significantly depending on the flow regime and geometry of the swimmer, as it is pointed in [13]. Generally, for slow swimming devices at low Reynolds numbers, the viscous forces become dominant. Hence, in this case, the Taylors resistive model is most applicable. For larger swimmers in which the added-mass effects dominate, Lighthill argues that reactive forces are the primary source of thrust and the resistive ones can be neglected. For, underwater snake robots, which lie in between these two extremes, both the resistive forces (drag forces) and reactive ones (added mass affects) need to be modeled, since both play a critical role in underwater swimming robotic systems propulsion (see e.g. [20]).

The force and moment balance equations require that the fluid terms have to be defined. However, it should be noted that the hydrodynamic forces (fluid forces) induced by the motion of a rigid body in an underwater environment are very complex and highly nonlinear. Consequently, we decided to solve the hydrodynamic modeling problem using an analytical simplified form suited for the design of online control of underwater snake robots. The Navier-Stokes equations are very difficult to solve and quite unsuited for robotics control design purposes. Hence, as far as the fluid effects are considered, for control design purposes, we need to model the hydrodynamic phenomena in a sufficiently simple manner while taking into account all the hydrodynamic effects that are significant for the control design.

It is important to notice that modeling for control design purposes poses different challenges than hydrodynamic modeling for simulations. In the latter, high accuracy and modeling of all hydrodynamic effects are important, while the model does not need to be in a form suited for analytical analysis. When modeling for model-based control design purposes, however, the model needs to be well suited for analytical analysis while only the significant hydrodynamic

effects need to be included. The closed-loop control system provides robustness to the less-significant unmodeled hydrodynamics, cf. for instance [21] and [22].

The literature provides three simple analytical models suitable for control design purposes. All of them are based on the fluid mechanics theory of slender bodies. The biomechanics community suggests the first one, the second one is offered by the oceanic engineering community and and the third one is a model that is mostly used in the robotics community.

In particular,

- the first model is a result of the Large Amplitude Elongated Body Theory (LAEBT) of fish locomotion by Lighthill [14],
- the second model is devoted to the dynamics of underwater flexible cables [12] and
- the third one is based on the Morison's equations and models the forces between the fluid and the cylindrical links of underwater snake robots [23], [24].

The underwater snake robotic system that is the subject of this paper, swims at a Reynolds number of approximately 10^4 to 10^5. As already mentioned, the models presented by Taylor [9] and Lighthill [14] are good candidates to model the fluid effects for slow swimmers at low Reynolds number and for fast swimmers at high Reynolds number, respectively. However, a detailed model of the fluid effects for Reynolds numbers of approximately 10^4 to 10^5 can only be achieved through a full numerical solution to the Navier-Stokes equations [13].

Unfortunately, the prohibitive computational costs of such methods are not suitable for real time control, and the resulting models would neither be suited for analytical analysis. In the modeling approach presented in this paper, we thus decide to use the Morison's equations [23], [24], assuming that the robot is a slender body. To quantify the fluid forces, each link of the underwater snake robot is considered as an isolated segment. Each segment of the robot is approximated as an elliptical cylinder. The fluid forces are modeled in each cross section of the links and depends only on the transverse link's motion. It is worth nothing that, in this modeling approach, the fluid effects that induced by the corners of the joints are neglected. We now present some assumptions underlying the modeling approach.

Assumption 1. The fluid is viscid, incompressible, and irrotational in the inertia frame.

Assumption 2. The robot is neutrally buoyant, i.e, we assume that the mass per unit of volume of the robot is equal to that of the water, such that gravity and buoyancy cancel each other out.

Assumption 3. The current in the inertial frame, $v_c = [V_{x,i}, V_{y,i}]^T$, is constant and irrotational.

Remark 1. Assumptions 1 and 2 are common assumptions in hydrodynamic modeling of slender body swimming robots [12], [13], [25], while Assumption 3 is a reasonable simplification of the real-world situation [22],[21].

Remark 2. Neutral buoyancy, ensuring that Assumption 2 is satisfied, is achieved by proper ballasting of the snake robot. The ballast will furthermore be positioned at the bottom of each snake robot link, in order to prevent it from rolling, making it self-stabilized in roll.

The fluid forces are functions of the current and it is shown in hydrodynamics literature, see e.g. [21], that the force exerted by the current can be characterized by the current velocity vector. This vector can be added vectorially to the link speed before calculating the fluid forces. In many works in ship control, in the presence of ocean currents the current is assumed to be constant in the body frame, i.e. it is assumed that $\dot{\mathbf{v}}_c = 0$. This assumption is easily violated during turning [21], and the current velocity should thus be assumed constant in the inertial frame, as given in Assumption 3.

The fluid forces will be expressed as functions of relative velocity, and thus the relative velocity of link i is defined as $v_{r,i}^{\text{link},i} = \dot{p}_i^{\text{link},i} - \mathbf{v}_{c,i}^{\text{link},i}$ [21], where $\mathbf{v}_{c,i}^{\text{link},i} = (\mathbf{R}_{\text{link},i}^{\text{global}})^T v_c = [v_{x,i}, v_{y,i}]^T$ is the current velocity expressed in body frame coordinates (F_B) and $v_c = [V_{x,i}, V_{y,i}]^T$ is the current velocity expressed in inertial frame coordinates (F_I). Due to Assumption 3 $\dot{v}_c = 0$ and thus

$$\dot{v}_{c,i}^{\text{link},i} = \frac{d}{dt}\left((\mathbf{R}_{\text{link},i}^{\text{global}})^T v_c\right) = \begin{bmatrix} -\sin\theta_i\dot{\theta}_i & \cos\theta_i\dot{\theta}_i \\ -\cos\theta_i\dot{\theta}_i & -\sin\theta_i\dot{\theta}_i \end{bmatrix} \begin{bmatrix} V_{x,i} \\ V_{y,i} \end{bmatrix} \quad (11)$$

As described by [13],[25], each link is subject to a force from the fluid acting on the CM of the link and also a fluid torque acting on the CM. In the following, we will derive the fluid forces and torques acting on the snake robot, using Morison's equations [23]. In particular, we will first state the assumption on which the development is based, then present how the force exerted by the fluid on a cylindrical object is made up of two components: the virtual mass force (added mass effect) and the drag force. The drag model that is employed here is in a form which takes into account the generalized case of anisotropic friction acting on each link. In particular, this means that each link has two drag coefficients, c_t and c_n, describing the drag force in the tangential (along link x axis) and normal (along link y axis) direction of the link, respectively. The fluid forces exerted on link i by the fluid can then be expressed as [23], [25]

$$f_i^{\text{link},i} = -\hat{\mathbf{C}}_A \dot{v}_{r,i}^{\text{link},i} - \hat{\mathbf{C}}_D v_{r,i}^{\text{link},i} - \hat{\mathbf{C}}_D \operatorname{sgn}\left(v_{r,i}^{\text{link},i}\right)\left(v_{r,i}^{\text{link},i}\right)^2, \quad (12)$$

where $\dot{v}_{r,i}^{\text{link},i} = \ddot{p}_i^{\text{link},i} - \dot{\mathbf{v}}_{c,i}^{\text{link},i}$ is the relative acceleration of link i, $\dot{p}_i^{\text{link},i}$ and $\ddot{p}_i^{\text{link},i}$ are the velocity and the acceleration of link i, respectively, expressed in the body frame, and $\hat{\mathbf{C}}_A$ and $\hat{\mathbf{C}}_D$ are constant diagonal (2×2) matrices depending on the shape of the body and the fluid characteristics. Moreover, it is worth to mention that the force expressions are formulated as functions of link x-coordinates, $df_i^{\text{link},i}(x)$, (see [23] and [24]) and then integrated over each body section to get the total force as:

$$f_i^{\text{link},i} = \int_{-l}^{l} df_i^{\text{link},i}(x) \quad (13)$$

Furthermore, we make the following assumption:

Assumption 4. The relative velocity at each section of the link in body-fixed frame (F_B) is equal to the relative velocity of the respective center of mass of each link. With this assumption we avoid the complexity of deriving the drag forces in analytical form, due to the nonlinear terms.

Remark 3. This approximation is valid in our case because the link's length is small compared to the total robot's length, which means that the velocities will not vary much from one section to the other. Furthermore, Assumption 4 let us avoid the numerical calculation of the drag forces due to the nonlinear terms.

Due to Assumption 4 it is not necessary to evaluate numerically the drag force and use an algorithmic approach of modeling, and thus we are able to derive a compact and closed form model of the underwater swimming robotic system.

We will now derive the matrices $\hat{\mathbf{C}}_D$ and $\hat{\mathbf{C}}_A$. For the cylindrical links with major diameter $2a$ and minor diameter $2b$ and taking into account that the length of each link is $2l$, we can express $\hat{\mathbf{C}}_D$, $\hat{\mathbf{C}}_A$ in this modeling approach as

$$\hat{\mathbf{C}}_D = \begin{bmatrix} c_t & 0 \\ 0 & c_n \end{bmatrix} = \begin{bmatrix} \frac{1}{2}\rho\pi C_f \frac{(b+a)}{2} 2l & 0 \\ 0 & \frac{1}{2}\rho C_D 2a 2l \end{bmatrix}, \tag{14}$$

$$\hat{\mathbf{C}}_A = \begin{bmatrix} \mu_t & 0 \\ 0 & \mu_n \end{bmatrix} = \begin{bmatrix} 0 & 0 \\ 0 & \rho\pi C_A a^2 2l \end{bmatrix}, \tag{15}$$

where C_f and C_D are the drag coefficients in x and y direction of motion, while C_A denotes the added mass coefficient [5], [26] and ρ is the density of the fluid. The added mass parameter in the x direction is considered equal to zero ($\mu_t = 0$), because the added mass of a slender body in longitudinal direction can be neglected compared to the body mass [26].

After modeling the fluid forces acting on the snake robot, we will now model the fluid moment τ_i. Many previous studies of underwater swimming robots neglect fluid torques, since it is assumed that they have little effect on the overall motion of the robot [11], [15]. In [13] a finite segment approach is employed in order to take into account the fluid moments, however, in this modeling approach the drag moment is evaluated numerically. Additionally, in [12] and [16] the fluid moments are taken into account but concluded in an algorithmic approach of computing the drag moment. We decide to include the fluid moments in the model because, first of all, this implies a more accurate modeling approach from a hydrodynamic perspective and, secondly, due to the fact that the fluid moments are directly related to the power consumption of the system. Since the fluid torques contribute significantly to the required actuation torques at the joints [13] and as the research on underwater swimming robots are expanding, there is increased demand for improved efficiency to allow for longer missions to be undertaken.

The fluid torque is a result of the link rotation only and thus the fluid torque on the CM of link i is a result of fluid forces acting normal to the link during link rotation. This approach is based on the common approach for a plate undergoing forced angular oscillation [27]. Each link of the robot is oscillating similarly to a flat plates oscillating in rotational motion. In [27] it is shown that under this assumption, the torque applied on link i by the fluid can be modeled through the relation

$$\tau_i = -\lambda_1 \ddot{\theta}_i - \lambda_2 \dot{\theta}_i - \lambda_3 \dot{\theta}_i |\dot{\theta}_i|, \tag{16}$$

where the λ_1, λ_2 and λ_3 parameters depend on the shape of the body and the fluid characteristics. It is worth mentioning that [27] shows that the parameter λ_2 can be set to zero, neglecting the torques due to the linear drag forces. Nevertheless, in our modeling approach we decide to consider, for completeness, the fluid torques due to the linear drag forces, since, these torques are dominant for slow swimming velocities.

We will now derive the fluid force parameters λ_1, λ_2 and λ_3. It is well-known that, for a cylinder, the added mass torque reduces to a simple analytical form with the parameter λ_1 expressed for a link with length $2l$ as [13], [25], [26]

$$\lambda_1 = \frac{1}{12}\rho\pi C_M (a^2 - b^2)^2 l^3, \tag{17}$$

where C_M is the added inertia coefficient. Additionally, in order to derive the parameters λ_2 and λ_3 we need to integrate the drag torque. As illustrated in Fig. 2, the drag force on an infinitesimal length of link i due to the link rotation, produces a drag torque about the CM of the link, which is given by

$$d\tau_{drag} = s df_{drag} = -sC_{Ld_x}\, s\dot{\theta}_i ds - sC_{Ld_x} \operatorname{sgn}\left(s\dot{\theta}_i\right)\left(s\dot{\theta}_i\right)^2 ds, \tag{18}$$

where s is the distance from the CM of link i to the element ds and $C_{Ld_x} = (1/2)\rho\pi C_f (b+a)/2$ [25]. Integrating (18), we can calculate the total drag torque on link i as

$$\tau_{drag} = -\int_{-l}^{l} \left(sC_{Ld_x}\, s\dot{\theta}_i + sC_{Ld_x} \operatorname{sgn}\left(s\dot{\theta}_i\right)\left(s\dot{\theta}_i\right)^2 \right) ds = -\lambda_2 \dot{\theta}_i - \lambda_3 \dot{\theta}_i |\dot{\theta}_i| \tag{19}$$

where λ_2 and λ_3 are given by

$$\lambda_2 = \frac{1}{6}\rho\pi C_f (a+b) l^3 \text{ and } \lambda_3 = \frac{1}{8}\rho\pi C_f (a+b) l^4 \tag{20}$$

The matrix $\hat{\mathbf{C}}_D$ and the parameters λ_2, λ_3 represent the drag forces parameters due to the pressure difference between the two sides of the body, while $\hat{\mathbf{C}}_A$ and λ_1 stand for the added mass of fluid carried by the moving body.

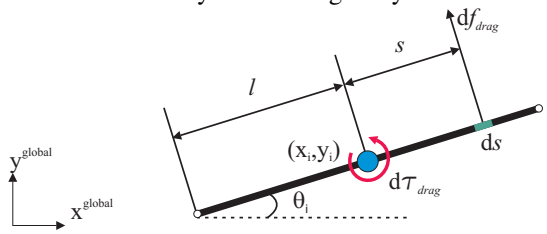

Fig. 2: The drag fluid torque about the CM of each link

We now will present the expression for the global frame fluid forces on link i. Using the transformation matrix we can express the global frame fluid forces on link i as:

$$f_i^{\text{global}} = \mathbf{R}_{\text{link},i}^{\text{global}} f_i^{\text{link},i} = \begin{bmatrix} \cos\theta_i & -\sin\theta_i \\ \sin\theta_i & \cos\theta_i \end{bmatrix} \begin{bmatrix} f_{x,i}^{\text{link},i} \\ f_{y,i}^{\text{link},i} \end{bmatrix}$$

$$= -\mathbf{R}_{\text{link},i}^{\text{global}} \hat{\mathbf{C}}_A \left((\mathbf{R}_{\text{link},i}^{\text{global}})^T \begin{bmatrix} \ddot{x}_i \\ \ddot{y}_i \end{bmatrix} - \begin{bmatrix} -\sin\theta_i \dot{\theta}_i & \cos\theta_i \dot{\theta}_i \\ -\cos\theta_i \dot{\theta}_i & -\sin\theta_i \dot{\theta}_i \end{bmatrix} \begin{bmatrix} V_{x,i} \\ V_{y,i} \end{bmatrix} \right)$$

$$- \mathbf{R}_{\text{link},i}^{\text{global}} \hat{\mathbf{C}}_D (\mathbf{R}_{\text{link},i}^{\text{global}})^T \begin{bmatrix} \dot{x}_i - V_{x,i} \\ \dot{y}_i - V_{y,i} \end{bmatrix} - \mathbf{R}_{\text{link},i}^{\text{global}} \hat{\mathbf{C}}_D \operatorname{sgn}\left(\begin{bmatrix} V_{r_x,i} \\ V_{r_y,i} \end{bmatrix} \right) \begin{bmatrix} V_{r_x,i}^2 \\ V_{r_y,i}^2 \end{bmatrix}, \tag{21}$$

where

$$\begin{bmatrix} V_{r_x,i} \\ V_{r_y,i} \end{bmatrix} = (\mathbf{R}_{\text{link},i}^{\text{global}})^T \begin{bmatrix} \dot{x}_i - V_{x,i} \\ \dot{y}_i - V_{y,i} \end{bmatrix}. \tag{22}$$

By performing the matrix multiplications and assembling the forces on all links in vector form, we can rewrite the global

frame fluid forces on the links as

$$\mathbf{f} = \begin{bmatrix} \mathbf{f_x} \\ \mathbf{f_y} \end{bmatrix} = \begin{bmatrix} \mathbf{f_{A_x}} \\ \mathbf{f_{A_y}} \end{bmatrix} + \begin{bmatrix} \mathbf{f}^{\mathrm{I}}_{\mathbf{D_x}} \\ \mathbf{f}^{\mathrm{I}}_{\mathbf{D_y}} \end{bmatrix} + \begin{bmatrix} \mathbf{f}^{\mathrm{II}}_{\mathbf{D_x}} \\ \mathbf{f}^{\mathrm{II}}_{\mathbf{D_y}} \end{bmatrix}, \tag{23}$$

where $\mathbf{f_{A_x}}$ and $\mathbf{f_{A_y}}$ represent the effects from added mass forces and are expressed as

$$\begin{aligned} \begin{bmatrix} \mathbf{f_{A_x}} \\ \mathbf{f_{A_y}} \end{bmatrix} = &- \begin{bmatrix} \mu_n(\mathbf{S}_\theta)^2 & -\mu_n \mathbf{S}_\theta \mathbf{C}_\theta \\ -\mu_n \mathbf{S}_\theta \mathbf{C}_\theta & \mu_n(\mathbf{C}_\theta)^2 \end{bmatrix} \begin{bmatrix} \ddot{\mathbf{X}} \\ \ddot{\mathbf{Y}} \end{bmatrix} \\ &- \begin{bmatrix} -\mu_n \mathbf{S}_\theta \mathbf{C}_\theta & -\mu_n(\mathbf{S}_\theta)^2 \\ \mu_n(\mathbf{C}_\theta)^2 & \mu_n \mathbf{S}_\theta \mathbf{C}_\theta \end{bmatrix} \begin{bmatrix} \mathbf{V}_x^a \\ \mathbf{V}_y^a \end{bmatrix} \dot{\theta}, \end{aligned} \tag{24}$$

where $\mathbf{V}_x^a = \mathrm{diag}(V_{x,1}, \ldots, V_{x,n}) \in \mathbb{R}^{n \times n}$ and $\mathbf{V}_y^a = \mathrm{diag}(V_{y,1}, \ldots, V_{y,n}) \in \mathbb{R}^{n \times n}$. The vectors $\mathbf{f}^{\mathrm{I}}_{\mathbf{D_x}}$, $\mathbf{f}^{\mathrm{I}}_{\mathbf{D_y}}$ and $\mathbf{f}^{\mathrm{II}}_{\mathbf{D_x}}$, $\mathbf{f}^{\mathrm{II}}_{\mathbf{D_y}}$ present the effects from the linear (25) and nonlinear drag forces (26), respectively, where the relative velocities are given from the Eq. 27.

$$\begin{bmatrix} \mathbf{f}^{\mathrm{I}}_{\mathbf{D_x}} \\ \mathbf{f}^{\mathrm{I}}_{\mathbf{D_y}} \end{bmatrix} = - \begin{bmatrix} c_t(\mathbf{C}_\theta)^2 + c_n(\mathbf{S}_\theta)^2 & (c_t - c_n)\mathbf{S}_\theta \mathbf{C}_\theta \\ (c_t - c_n)\mathbf{S}_\theta \mathbf{C}_\theta & c_t(\mathbf{S}_\theta)^2 + c_n(\mathbf{C}_\theta)^2 \end{bmatrix} \begin{bmatrix} \dot{\mathbf{X}} - \mathbf{V}_x \\ \dot{\mathbf{Y}} - \mathbf{V}_y \end{bmatrix} \tag{25}$$

$$\begin{bmatrix} \mathbf{f}^{\mathrm{II}}_{\mathbf{D_x}} \\ \mathbf{f}^{\mathrm{II}}_{\mathbf{D_y}} \end{bmatrix} = - \begin{bmatrix} c_t \mathbf{C}_\theta & -c_n \mathbf{S}_\theta \\ c_t \mathbf{S}_\theta & c_n \mathbf{C}_\theta \end{bmatrix} \mathrm{sgn}\left(\begin{bmatrix} \mathbf{V_{r_x}} \\ \mathbf{V_{r_y}} \end{bmatrix} \right) \begin{bmatrix} \mathbf{V_{r_x}}^2 \\ \mathbf{V_{r_y}}^2 \end{bmatrix} \tag{26}$$

$$\begin{bmatrix} \mathbf{V_{r_x}} \\ \mathbf{V_{r_y}} \end{bmatrix} = \begin{bmatrix} \mathbf{C}_\theta & \mathbf{S}_\theta \\ -\mathbf{S}_\theta & \mathbf{C}_\theta \end{bmatrix} \begin{bmatrix} \dot{\mathbf{X}} - \mathbf{V}_x \\ \dot{\mathbf{Y}} - \mathbf{V}_y \end{bmatrix} \tag{27}$$

In addition, the fluid torques on all links in matrix form are

$$\tau = -\Lambda_1 \ddot{\theta} - \Lambda_2 \dot{\theta} - \Lambda_3 \dot{\theta} |\dot{\theta}|, \tag{28}$$

where $\Lambda_1 = \lambda_1 \mathbf{I}_n$, $\Lambda_2 = \lambda_2 \mathbf{I}_n$ and $\Lambda_3 = \lambda_3 \mathbf{I}_n$.

D. Equations of motion

This section presents the equations of motion for the underwater snake robot. The forces and torques acting on link i are visualized in Fig. 1b and the force balance for link i in global frame coordinates is given by

$$m\ddot{x}_i = h_{x,i} - h_{x,i-1} + f_{x,i}, \quad m\ddot{y}_i = h_{y,i} - h_{y,i-1} + f_{y,i} \tag{29}$$

The force balance equations for all links may be expressed in matrix form as

$$m\ddot{\mathbf{X}} = \mathbf{D}^T \mathbf{h}_x + \mathbf{f_x}, \quad m\ddot{\mathbf{Y}} = \mathbf{D}^T \mathbf{h}_y + \mathbf{f_y}. \tag{30}$$

Note that the link accelerations may also be expressed by differentiating (6) twice with respect to time. This gives

$$\mathbf{D}\ddot{\mathbf{X}} = l\mathbf{A}\left(\mathbf{C}_\theta \dot{\theta}^2 + \mathbf{S}_\theta \ddot{\theta}\right), \quad \mathbf{D}\ddot{\mathbf{Y}} = l\mathbf{A}\left(\mathbf{S}_\theta \dot{\theta}^2 - \mathbf{C}_\theta \ddot{\theta}\right). \tag{31}$$

We obtain the acceleration of the CM by differentiating (4) twice with respect to time, inserting (30), and noting that the constraint forces $\mathbf{h}_x$ and $\mathbf{h}_y$, are cancelled out when the link accelerations are summed. This gives

$$\begin{bmatrix} \ddot{p}_x \\ \ddot{p}_y \end{bmatrix} = \frac{1}{n} \begin{bmatrix} \mathbf{e}^T \ddot{\mathbf{X}} \\ \mathbf{e}^T \ddot{\mathbf{Y}} \end{bmatrix} = \frac{1}{nm} \begin{bmatrix} \mathbf{e}^T & \mathbf{0}_{1\times n} \\ \mathbf{0}_{1\times n} & \mathbf{e}^T \end{bmatrix} \mathbf{f} \tag{32}$$

This equation simply states, as would be expected, that the acceleration of the CM of an underwater snake robot equals the sum of the external forces acting on the robot divided by its mass. The torque balance for link i is given by

$$J\ddot{\theta}_i = u_i - u_{i-1} - l\sin\theta_i (h_{x,i} + h_{x,i-1}) + l\cos\theta_i \left(h_{y,i} + h_{y,i-1}\right) + \tau_i. \tag{33}$$

Hence, the torque balance equations for all links may be expressed in matrix form as

$$\mathbf{J}\ddot{\theta} = \mathbf{D}^T \mathbf{u} - l\mathbf{S}_\theta \mathbf{A}^T \mathbf{h}_x + l\mathbf{C}_\theta \mathbf{A}^T \mathbf{h}_y + \tau, \tag{34}$$

where τ is given from (28). What now remains is to remove the constraint forces from (34). Premultiplying (30) by $\mathbf{D}$ and solving for $\mathbf{h}_x$ and $\mathbf{h}_y$, we can write the expression for the joint constraint forces as

$$\begin{aligned} \mathbf{h}_x = &(\mathbf{D}\mathbf{D}^T)^{-1}\mathbf{D}(m\ddot{\mathbf{X}} + \mu_n(\mathbf{S}_\theta)^2 \ddot{\mathbf{X}} - \mu_n \mathbf{S}_\theta \mathbf{C}_\theta \ddot{\mathbf{Y}} \\ &- \mu_n \mathbf{S}_\theta \mathbf{C}_\theta \mathbf{V}_x^a \dot{\theta} - \mu_n(\mathbf{S}_\theta)^2 \mathbf{V}_y^a \dot{\theta} - \mathbf{f}^{\mathrm{I}}_{\mathbf{D_x}} - \mathbf{f}^{\mathrm{II}}_{\mathbf{D_x}}) \\ \mathbf{h}_y = &(\mathbf{D}\mathbf{D}^T)^{-1}\mathbf{D}(m\ddot{\mathbf{Y}} - \mu_n \mathbf{S}_\theta \mathbf{C}_\theta \ddot{\mathbf{X}} + \mu_n(\mathbf{C}_\theta)^2 \ddot{\mathbf{Y}} \\ &+ \mu_n(\mathbf{C}_\theta)^2 \mathbf{V}_x^a \dot{\theta} + \mu_n \mathbf{S}_\theta \mathbf{C}_\theta \mathbf{V}_y^a \dot{\theta} - \mathbf{f}^{\mathrm{I}}_{\mathbf{D_y}} - \mathbf{f}^{\mathrm{II}}_{\mathbf{D_y}}). \end{aligned} \tag{35}$$

Inserting in Eq. (34) the joint constraints forces Eq. (35) and also replacing $\mathbf{D}\ddot{\mathbf{X}}$, $\mathbf{D}\ddot{\mathbf{Y}}$ with (31) and $\ddot{\mathbf{X}}$,$\ddot{\mathbf{Y}}$ with (10), and solving for $\ddot{\theta}$, we can finally rewrite the modeling of an underwater snake robot as

$$\mathbf{M}_\theta \ddot{\theta} + \mathbf{W}_\theta \dot{\theta}^2 + \mathbf{V}_\theta \dot{\theta} + \Lambda_3 |\dot{\theta}| \dot{\theta} - l\mathbf{S}_\theta \mathbf{K}\mathbf{f_{Dx}} + l\mathbf{C}_\theta \mathbf{K}\mathbf{f_{Dy}} = \mathbf{D}^T \mathbf{u}, \tag{36}$$

where $\mathbf{f_{Dx}} = \mathbf{f}^{\mathrm{I}}_{\mathbf{D_x}} + \mathbf{f}^{\mathrm{II}}_{\mathbf{D_x}}$ and $\mathbf{f_{Dy}} = \mathbf{f}^{\mathrm{I}}_{\mathbf{D_y}} + \mathbf{f}^{\mathrm{II}}_{\mathbf{D_y}}$ are the drag forces in x and y directions, respectively, and $\mathbf{M}_\theta$, $\mathbf{W}_\theta$ and $\mathbf{V}_\theta$ are defined as

$$\begin{aligned} \mathbf{M}_\theta = &\mathbf{J} + ml^2 \mathbf{S}_\theta \mathbf{V} \mathbf{S}_\theta + ml^2 \mathbf{C}_\theta \mathbf{V} \mathbf{C}_\theta + \Lambda_1 + l^2 \mathbf{S}_\theta \mathbf{K} \mu_n (\mathbf{S}_\theta)^2 \mathbf{H} \mathbf{S}_\theta \\ &+ l^2 \mathbf{S}_\theta \mathbf{K} \mu_n \mathbf{S}_\theta \mathbf{C}_\theta \mathbf{H} \mathbf{C}_\theta + l^2 \mathbf{C}_\theta \mathbf{K} \mu_n \mathbf{S}_\theta \mathbf{C}_\theta \mathbf{H} \mathbf{S}_\theta + l^2 \mathbf{C}_\theta \mathbf{K} \mu_n (\mathbf{C}_\theta)^2 \mathbf{H} \mathbf{C}_\theta \end{aligned} \tag{37}$$

$$\begin{aligned} \mathbf{W}_\theta = &ml^2 \mathbf{S}_\theta \mathbf{V} \mathbf{C}_\theta - ml^2 \mathbf{C}_\theta \mathbf{V} \mathbf{S}_\theta + l^2 \mathbf{S}_\theta \mathbf{K} \mu_n (\mathbf{S}_\theta)^2 \mathbf{H} \mathbf{C}_\theta \\ &- l^2 \mathbf{S}_\theta \mathbf{K} \mu_n \mathbf{S}_\theta \mathbf{C}_\theta \mathbf{H} \mathbf{S}_\theta + l^2 \mathbf{C}_\theta \mathbf{K} \mu_n \mathbf{S}_\theta \mathbf{C}_\theta \mathbf{H} \mathbf{C}_\theta - l^2 \mathbf{C}_\theta \mathbf{K} \mu_n (\mathbf{C}_\theta)^2 \mathbf{H} \mathbf{S}_\theta \end{aligned} \tag{38}$$

$$\begin{aligned} \mathbf{V}_\theta = &\Lambda_2 - l\mathbf{S}_\theta \mathbf{K} \mu_n \mathbf{S}_\theta \mathbf{C}_\theta \mathbf{V}_x^a - l\mathbf{S}_\theta \mathbf{K} \mu_n (\mathbf{S}_\theta)^2 \mathbf{V}_y^a - l\mathbf{C}_\theta \mathbf{K} \mu_n (\mathbf{C}_\theta)^2 \mathbf{V}_x^a \\ &- l\mathbf{C}_\theta \mathbf{K} \mu_n \mathbf{S}_\theta \mathbf{C}_\theta \mathbf{V}_y^a \end{aligned} \tag{39}$$

The equations of motion for the underwater snake robot are in other words given by (32) and (36). By introducing the state variable $\mathbf{x} = \left[\theta^T, \mathbf{p}_{CM}^T, \dot{\theta}^T, \dot{\mathbf{p}}_{CM}^T\right]^T \in \mathbb{R}^{2n+4}$, we can rewrite the model of the underwater snake like robot compactly in state space form as

$$\dot{\mathbf{x}} = \left[\dot{\theta}^T, \dot{\mathbf{p}}_{CM}^T, \ddot{\theta}^T, \ddot{\mathbf{p}}_{CM}^T\right]^T = \mathbf{F}(\mathbf{x}, \mathbf{u}) \tag{40}$$

where the elements of $\mathbf{F}(\mathbf{x}, \mathbf{u})$ are easily found by solving (32) and (36) for $\ddot{\mathbf{p}}_{CM}$ and $\ddot{\theta}$, respectively.

Remark 4. It is interesting to note that if, in the dynamic model (32) and (36), we set the fluid parameters to zero and replace the drag forces in x and y direction with ground friction models [19], then the model reduces to an identical dynamic model of a ground snake robot, described in [19]. The underwater snake robot model is thus an extension of the land snake robot model, and may be used for amphibious snake robots moving both on land and in water.

III. SIMULATION RESULTS

In this section, simulation results will be presented for three different modeling approaches: **case 1** – Added mass and nonlinear drag effect, **case 2** – Added mass, linear and nonlinear drag effect and **case 3** – Added mass, linear drag effect, nonlinear drag effect and current effect. In the following, the mathematical expressions for lateral undulation and eel-like motion are presented. Moreover, we explain how to choose the fluid parameters. Finally, the simulation results are presented for both lateral undulation and eel-like motion. The models were implemented in *Matlab R2011b*. The dynamics was calculated using the *ode23tb* solver with a relative and absolute error tolerance of 10^{-4}.

A. Lateral undulation

The mathematical expression for the snake's gait in locomotion studies depends on its construction and model. Lateral undulation [1] is the fastest and most common form

of snake locomotion, where the motion is achieved by creating continuous body waves that are propagated backwards from head to tail. In order to achieve lateral undulation, the snake is commanded to follow the serpenoid curve [3]. The proposed lateral undulation is realized by controlling each joint of the snake robot according to the sinusoidal reference

$$\phi_i^* = \alpha \sin(\omega t + (i-1)\beta) + \gamma, \quad i = 1, \ldots, n-1, \tag{41}$$

where the parameter α corresponds to the amplitude of the serpentine wave that propagates along the body of the snake robot, ω is the angular frequency of the sinusoidal joint motion, β determines the phase shift between the sequential joints, and γ is the joint offset that is used to control the direction of the motion.

B. Eel-like motion

Eel-like motion is achieved by propagating lateral axial undulations with increasing amplitude from nose to tail [8]. A simple equation is derived for the eel-like motion by controlling each joint of the snake robot according to the reference signal

$$\phi_i^* = \alpha \left(\frac{n-i}{n+1} \right) \sin(\omega t + (i-1)\beta) + \gamma, \quad i = 1, \ldots, n-1, \tag{42}$$

where the parameter $\alpha(n-i)/(n+1)$ corresponds to the increasing amplitude, from nose to tail, of the wave that propagates along the body of the snake robot, ω is the angular frequency of the sinusoidal joint motion, β determines the phase shift between the joints, and γ is the joint offset.

C. Low-level joint control

A standard PD-controller is used to calculate the joints' actuator torques from the joints' reference angles according to

$$u_i = K_{p,i}(\phi_i^* - \phi_i) - K_{d,i}\dot{\phi}_i, \quad i = 1, \ldots, n-1, \tag{43}$$

where $K_{p,i} > 0$ and $K_{d,i} > 0$ are the gains of the controller. A velocity reference is not included in (43) since the purpose of the derivative part is simply to damp the joint motion, if the joint velocities become large. The advantage of this controller is that it does not require calculation of the derivative of ϕ_i^* with respect to time, while its disadvantage is that it is unable to track time-varying joint reference angles perfectly.

D. Fluid parameters

As already mentioned, in our modeling approach, we decide to use Morison's equation assuming that each link of the robot is an elliptical cylinder. Hence, it is important to investigate the influence of the current effects on cylindrical objects. Even though the force coefficients vary very much in the presence of current, Sarpkaya and Storm [28] found a modified Morison equation to represent the measured force in a coexisting flow field as well as the original equation in a no-current field.

It must be noted that, ideally, the drag and added mass coefficients of the system should be determined experimentally. This information is not available and the coefficients will be chosen under the assumption of a steady-state flow [20], [16]. The added mass coefficients are simply set to their theoretical values, $C_A = 1$ and $C_M = 1$ [13]. In [29], Guskova et al. investigate the C_D and C_A of laterally oscillating elliptical cylinders under conditions dimensionally equivalent to those of our underwater snake robot. The parameter C_D is found to vary from approximately 2 to 3 and C_A varies between 0.93 and 1. In [29], it is mentioned that the lateral coefficients of the simulated robot may not deviate significantly from their steady-state values. In our simulations, we decide to apply the steady-state coefficients. The axial viscous force's coefficient is selected as $C_f = 0.03$ from a review of experimental data presented in [30]. In addition, for a cylindrical obstacle immerged in a flow with a Reynolds number of approximately $R_e \simeq 10^5$, the fluid parameters can be set as $C_D = 1$, $C_A = 1$, $C_f = 0.01$, $C_M = 1$ [16].

E. Simulation parameters

A snake robot was considered with $n = 10$ links, each one having length $2l = 2 \times 0.14$ m. The mass of each link is $m = 0.6597$ kg and is chosen so to fulfil the neutrally buoyant assumption. The initial values of the states of the snake robot were set to zero, i.e. the snake robot is initially at rest at the origin, with its heading along the inertial x axis. The hydrodynamic related parameters for the elliptic section with half small and great axis' length 0.03 m and 0.05 m, respectively, $\rho = 1000$ kg/m^3, $C_f = 0.03$, $C_D = 2$, $C_A = 1$ and $C_M = 1$ were chosen as: $\hat{\mathbf{C}}_D = \text{diag}[0.2639 \quad 8.4]$, $\hat{\mathbf{C}}_A = \text{diag}[0 \quad 0.3958]$, $\lambda_1 = 4.3103 \times 10^{-4}$, $\lambda_2 = 2.2629 \times 10^{-5}$, $\lambda_3 = 2.2988 \times 10^{-7}$. It should be noted that the anisotropic friction property is achieved by a low drag coefficient in the tangential direction and a higher one in the perpendicular. The values of a constant current in inertial frame are set to $[0.1, 0.1]$ m/sec. In this simulation a joint PD-controller (43) is used with parameters $K_p = 200, K_d = 50$, while lateral undulation or eel-like motion are achieved by moving the joints according to the (41) or (42), respectively, with gait parameters $\alpha = 30^o$, $\beta = 30^o$, $\omega = 70^o/\text{sec}$ and $\gamma = 0^o$.

F. Lateral undulation: simulation results

In this section, we let the snake robot move by the motion pattern of lateral undulation (41). We include this motion pattern since it is commonly used for ground snake robots, and we therefore, want to show how this (forward) motion is obtained by an underwater snake robot. Simulation results for lateral undulation of the underwater snake robot is presented for the three different cases. In particular, the motion of the center of mass is presented in Fig. 3a and the forward velocity (5) is presented in Fig. 3b. It should be noted that the robot is is moving in a straight line in **case 3**, although the presence of current.

G. Eel-like motion: simulation results

In this section, we present and compare the simulation results for the eel-like motion pattern for the three different cases. In particular, the motion of the center of mass is presented in Fig. 4a and the forward velocity is presented in Fig. 4b. In contrast to the lateral undulation, the robot is moving almost in a straight line in **case 3**, although the

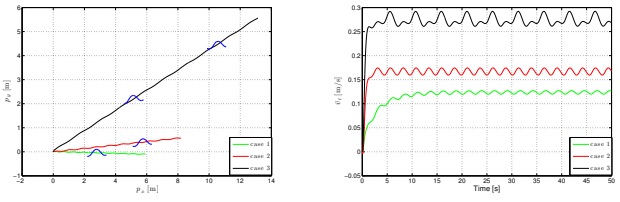

(a) Position of the CM (b) Velocity of the CM

Fig. 3: Simulation results for lateral undulation

presence of current (Fig. 4a). A more efficient way for eel-like motion pattern have to be analysed, in the future, in order to mimic exactly the biological motion of eels and also take into account the power consumption.

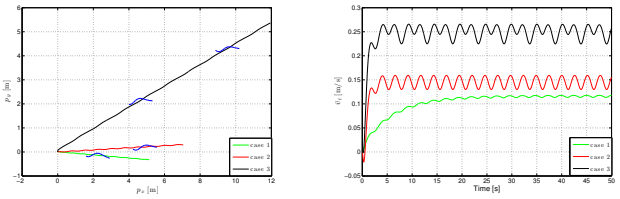

(a) Position of the CM (b) Velocity of the CM

Fig. 4: Simulation results for eel-like motion

IV. CONCLUSIONS AND FUTURE WORK

This paper has presented a model of the kinematics and dynamics of a planar, underwater snake robot. The model is in closed-loop form and is thus particularly well suited for modern model-based control design schemes. As it is mentioned before, the fluid forces induced by the motion of a rigid body in an underwater environment are very complex and highly nonlinear and therefore several of these effects are often not taken into account when modeling the system. In this modeling approach, however, the combination of linear and the nonlinear drag forces, the added mass effect, the fluid moments and current effect are considered. Simulation results for the serpentine motion pattern for lateral undulation and eel-like motion are presented. In future work, the authors will employ the proposed model in order to develop and analyze controllers for underwater snake robot. In addition, an extension of the modeling in any 2D plane of 3D will be investigated in order to provide the ability to use it for depth control purposes in the future.

ACKNOWLEDGMENT

The authors thank O. M. Faltinsen, T. I. Fossen and Zhao He for the very helpful and significant comments and suggestions with regards to the hydrodynamic modeling.

REFERENCES

[1] P. Liljebäck, K. Y. Pettersen, Ø. Stavdahl, and J. T. Gravdahl, "A review on modelling, implementation, and control of snake robots," *Robotics and Autonomous Systems*, vol. 60, pp. 29–40, 2012.

[2] J. Gray, "Studies in animal locomotion," *Journal of Experimental Biology*, vol. 10, no. 1, pp. 88–104, 1933.

[3] S. Hirose, *Biologically Inspired Robots: Snake-Like Locomotors and Manipulators*. Oxford: Oxford University Press, 1993.

[4] A. Crespi, A. Badertscher, A. Guignard, and A. Ijspeert, "Swimming and crawling with an amphibious snake robot," in *Proceedings of the IEEE International Conference on Robotics and Automation (ICRA 2005).*, April 2005, pp. 3024 – 3028.

[5] F. Boyer, D. Chablat, P. Lemoine, and P. Wenger, "The eel-like robot," *CoRR*, vol. abs/0908.4464, 2009.

[6] H. Yamada, S. Chigisaki, M. Mori, K.Takita, K. Ogami, and S. Hirose, "Development of amphibious snake-like robot ACM-R5," in *Proc. 36th Int. Symp. Robotics*, 2005.

[7] I. Borazjani and F. Sotiropoulos, "On the role of form and kinematics on the hydrodynamics of self-propelled body/caudal fin swimming," *Experimental Biology*, vol. 217, p. 89107, 2010.

[8] J. Colgate and K. Lynch, "Mechanics and control of swimming: a review," *IEEE Journal of Oceanic Engineering*, vol. 29, no. 3, pp. 660 – 673, July 2004.

[9] G. Taylor, "Analysis of the swimming of long and narrow animals," *Proceedings of the Royal Society of London. Series A. Mathematical and Physical Sciences*, vol. 214, no. 1117, pp. 158–183, 1952.

[10] E. Tytell, "The hydrodynamics of eel swimming: II. effect of swimming speed," *J Exp. Biol.*, vol. 207, pp. 3265–3279, 2004.

[11] K. McIsaac and J. Ostrowski, "Motion planning for anguilliform locomotion," *IEEE Trans. Rob. Aut.*, vol. 19, no. 4, pp. 637–625, 2003.

[12] F. Boyer, M. Porez, and W. Khalil, "Macro-continuous computed torque algorithm for a three-dimensional eel-like robot," *IEEE Transactions on Robotics*, vol. 22, no. 4, pp. 763 –775, aug. 2006.

[13] A. Wiens and M. Nahon, "Optimally efficient swimming in hyper-redundant mechanisms: control, design, and energy recovery." *Bioinspir Biomim*, vol. 7, no. 4, p. 046016, 2012.

[14] M. J. Lighthill, "Large-amplitude elongated-body theory of fish locomotion," *Proceedings of the Royal Society of London. Series B. Biological Sciences*, vol. 179, no. 1055, pp. 125–138, 1971.

[15] O. Ekeberg, "A combined neuronal and mechanical model of fish swimming," *Biological Cybernetics*, vol. 69, pp. 363–374, 1993, 10.1007/BF00199436.

[16] W. Khalil, G. Gallot, and F. Boyer, "Dynamic modeling and simulation of a 3-d serial eel-like robot," *Systems, Man, and Cybernetics, Part C: Applications and Reviews, IEEE Transactions on*, vol. 37, no. 6, pp. 1259 –1268, nov. 2007.

[17] F. Candelier, M. Porez, and F. Boyer, "Note on the swimming of an elongated body in a non-uniform flow," *Journal of Fluid Mechanics*, vol. 716, pp. 616–637, 2 2013.

[18] F. Boyer, M. Porez, A. Leroyer, and M. Visonneau, "Fast dynamics of an eel-like robot-comparisons with navier-stokes simulations," *IEEE Transactions on Robotics*, vol. 24, no. 6, pp. 1274–1288, 2008.

[19] P. Liljebäck, K. Pettersen, Ø. Stavdahl, and J. T. Gravdahl, *Snake Robots: Modelling, Mechatronics, and Control*, Springer-Verlag, Ed. Advances in Industrial Control, 2013.

[20] C. Jordan, "Coupling internal and external mechanics to predict swimming behavior: A general approach," *American Zoologist*, vol. 36, no. 6, pp. 710–722, 1996.

[21] T. I. Fossen, *Motion Control Systems*. John Wiley & Sons, Ltd, 2011.

[22] S. Fan and C. Woolsey, "Underwater vehicle control and estimation in nonuniform currents," in *American Control Conference*, Washington, DC, June 17-19 2013.

[23] J. Morison, J. Johnson, and S. Schaaf, "The force exerted by surface waves on piles," *Journal of Petroleum Technology*, vol. 2, pp. 149–154, May 1950.

[24] O. M. Faltinsen, *Sea loads on ships and offshore structures / O.M. Faltinsen*. Cambridge University Press Cambridge ; New York, 1990.

[25] W. Khalil, G. Gallot, O. Ibrahim, and F. Boyer, "Dynamic modeling of a 3-d serial eel-like robot," in *Robotics and Automation, 2005. ICRA 2005. Proceedings of the 2005 IEEE International Conference on*, april 2005, pp. 1270 – 1275.

[26] J. Newman, *Marine Hydrodynamics*. MIT Press, 1977.

[27] K. Klaka, J. Penrose, R. Horsley, and M. Renilson, "Hydrodynamic tests on a plate in forced oscillation," *Ocean Engineering*, vol. 34, no. 89, pp. 1225 – 1234, 2007.

[28] T. Sarpkaya and M. Storm, "In-line force on a cylinder translating in oscillatory flow," *Applied Ocean Research*, vol. 7, no. 4, pp. 188–196, October 1985.

[29] N. Y. Guskova, G. V. Makhortykh, and M. G. Shcheglova, "Inertia and drag of elliptic cylinders oscillating in a fluid," *Fluid Dynamics*, vol. 33, pp. 91–95, 1998.

[30] M. P. Païdoussis, "8 solitary cylindrical structures in axial flow," in *Slender Structures and Axial Flow*, ser. Fluid-Structure Interactions. Academic Press, 2003, vol. 2, pp. 787 – 1032.